SAND2015-9115C

Modal Testing of a Nose Cone using Three-Dimensional Scanning Laser Doppler Vibrometry

Daniel P. Rohe
Structural Dynamics & X-ray/NDE Department
Sandia National Laboratories*
P.O. Box 5800 - MS0557
Albuquerque, NM, 87185
dprohe@sandia.gov

ABSTRACT

The Structural Dynamics department at Sandia National Laboratories has acquired a 3D Scanning Laser Doppler Vibrometer system for making vibration and modal test measurements. This paper presents the results of testing performed to examine the capabilities and limitations of that system. The test article under consideration was a conical part with two different surface materials which allowed the examination of the effect of angle of incidence and surface reflectivity on the measurement. The system was operated in both 1D and 3D modes, and the results from the 1D scan were compared to a scan performed with a previous generation system to evaluate the improvements between the generations. Data from the laser systems were exported to standard curve fitting software, and modes were fit to the data.

Keywords: 3D, SLDV, Alignment, Incidence, Modal

1 INTRODUCTION

Scanning Laser Doppler Vibrometry (SLDV) has been shown to have advantages over traditional mounted sensors [1]. For example, it allows for non-contact measurements which do not mass-load the test article. Additionally, a finer measurement point resolution can often be achieved through the use of scanning mirrors in the laser heads which are much more precise than a roving hammer or roving accelerometer test. The Structural Dynamics department at Sandia National Laboratories has owned and operated a Polytec PSV-400 1D SLDV system for several years, and during that time identified a number of limitations with the 1D SLDV system. The 1D system always measures in the direction of the beam, which limits the measurement of in-plane motions. It was also subject to unfamiliar (at least from the point of view of a modal engineer) optical issues such as signal dropouts, visibility minima, and speckle noise. These issues limited the use of the system for general-purpose or production testing.

To improve the SLDV capability at Sandia National Laboratories, a Polytec PSV-500 3D SLDV system was recently purchased. The 3D system has the obvious advantage of being able to produce three-dimensional measurements at each measurement point. These full-field measurements can then be used to perform more complex operations such as computing strain. Additionally, the SLDV hardware improved significantly between the purchase of the two systems, which can limit some of the unfamiliar optical issues. The goal of this effort was to gain experience using the 3D SLDV system and compare it to the previous 1D SLDV system for general modal testing.

2 TEST DESCRIPTIONS

To examine the capabilities and limitations of the 3D SLDV system, a series of modal test were performed on a conical test article, shown in Figure 1. The test article was chosen because it had both dark and light surfaces which would allow

* Sandia National Laboratories is a multi-program laboratory managed and operated by Sandia Corporation, a wholly owned subsidiary of Lockheed Martin Corporation, for the U.S. Department of Energy's National Nuclear Security Administration under contract DE-AC04-94AL85000

comparison of signal return, and its conical shape would allow investigation of the angle of incidence (AoI) of the laser beam on the quality of the data.

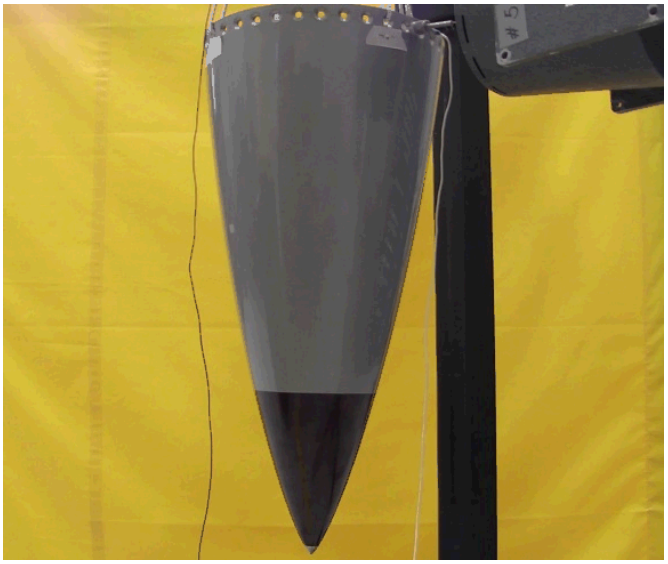

Figure 1: Conical test article

The part was tested using three different measurement configurations. The first test used the previous generation 1D SLDV system; this will be referred to throughout this work as the baseline test. The second test used the newer system in a 1D configuration (only utilizing one of the three scanning heads), and the third test used the newer system in 3D configuration (utilizing all three scanning heads). By performing 1D tests with both SLDV systems, a more accurate estimate of the hardware improvements could be obtained. To ensure consistent points were scanned for meaningful comparisons between tests, a test grid was created with 10 axial stations and 16 circumferential stations. The coordinates for each scan point were derived from drawings of the part, with the global *x* axis along the axis of revolution of the test article. This geometry is shown in Figure 2.

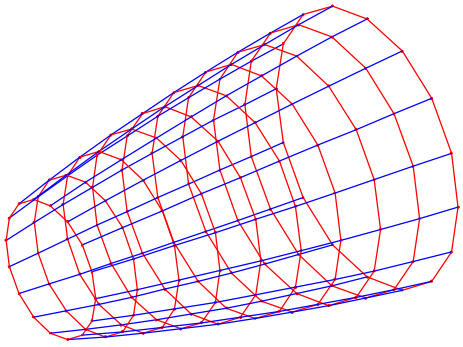

Figure 2: Test geometry created to ensure consistent scan points between tests.

In order to point at measurement locations on the part defined by geometry, the lasers first needed to be aligned with the part coordinate system. The alignment procedure was complicated by the lack of sharp features on the part where coordinates were known: the only features available for alignment were the tip of the test article and the ring of holes near the base. The coordinates of these features were extracted from drawings, but there was a significant amount of uncertainty in positioning the lasers at these features: the lasers cannot point at a hole, so some point around the hole needed to be selected. For this test, the point was placed at the boundary of the countersink closest to the tip of the test article. Figure 3 shows example laser alignments at features on the test article.

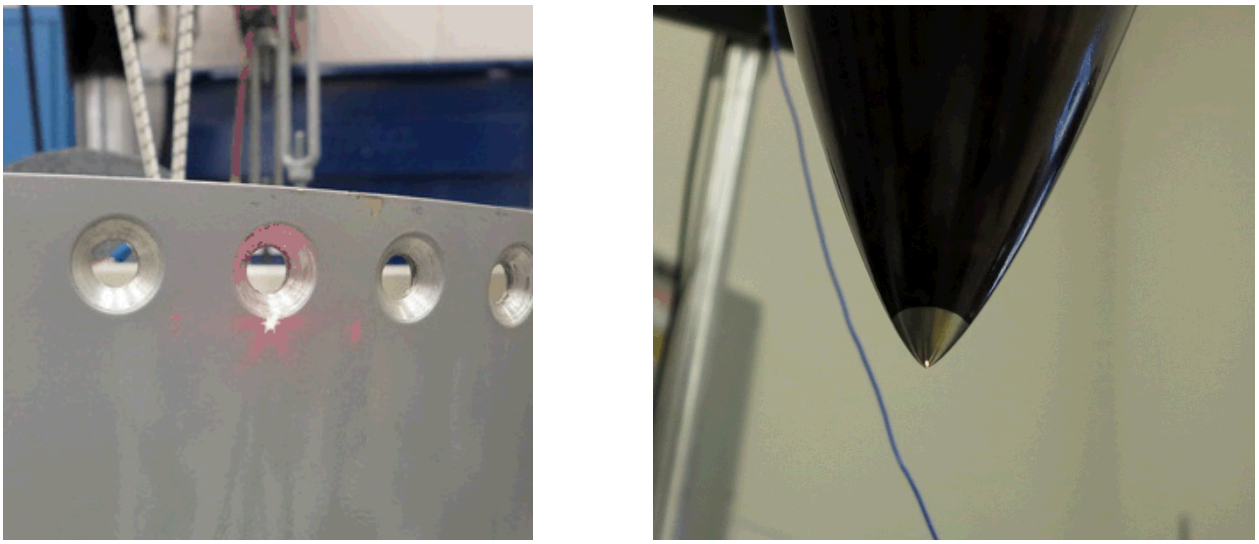

Figure 3: Positioning the laser spots at features on the test article for alignment

2.1 Baseline Test

The baseline test was set up using the 1D laser system as shown in Figure 4. The laser head was positioned approximately 1.35 meters (53.1 in) from the test article, which was suspended on soft bungee cords. A modal shaker and force transducer were attached to the exterior of the part at the same axial position as the ring of holes, and a drive point accelerometer was mounted on the interior of the test article directly aligned with the force transducer.

Figure 4: Baseline test setup

Since the laser requires line-of-sight to a point to make a measurement, multiple scans were needed to measure all sides of the test article. For each scan, the laser head was aligned with the test article's coordinate system using the features described in Section 2, generally using four or five holes and the tip of the test article for alignment. Figure 5 shows an example of the alignment points used for one scan. The error in the alignment calculated by the laser system was on average 1.3 mm; compared to the grid spacing of 50-60 mm, it was thought that this error was acceptable. With the lasers aligned, the geometry could be imported and reduced to the points visible from that scan direction. Figure 6 shows an example of the measurement points. The baseline system struggled to measure more than four circumferential stations in one scan due to poor signal return from the high AoI. The maximum AoI for a measured point in this test was 55 degrees. With 16 circumferential stations, this required four separate scans to measure the entire part with each scan measuring 40 points.

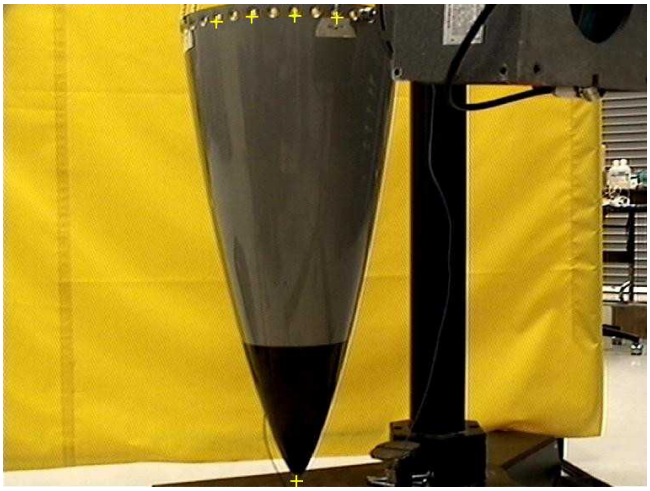

Figure 5: Laser camera view showing points used for alignment (marked with +).

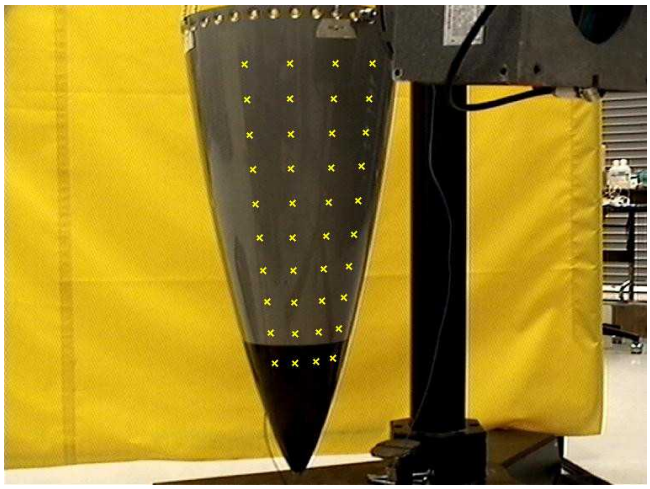

Figure 6: Laser camera view showing measurement points for a given baseline scan.

Frequency response functions (FRFs) were measured up to 2,000 Hz with a frequency resolution of 1.25 Hz. Random excitation was applied to the shaker and 20 averages were measured at each scan point. Hann windows were applied to the measured responses. For this test, all signal enhancement parameters were set to their highest levels. This allowed the laser system to detect when poor quality data were measured and add up to 100 total averages to improve the data.

It became obvious during the test that the baseline system was struggling to get good measurements from the darker surface due to poor signal return. Signal dropouts and their resulting over-ranges were prevalent. The system was not able to measure FRFs for 10 of the 16 points on the darker surface, and the FRFs of the points that were measured were very noisy (see, for example, Figure 7).

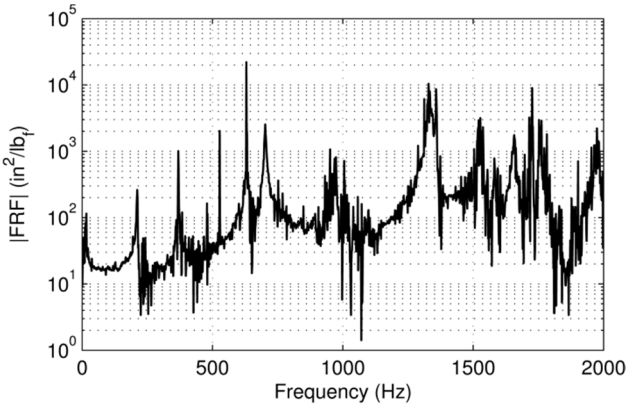

Figure 7: Example FRF from darker surface with an AoI of 41 degrees.

2.2 1D Test with New System

The same test article was scanned with the new system in 1D mode to compare the results to the previous test. Due to lab space constraints, the original test setup had to be dismantled between tests, but the shaker hardware was left attached to the test article to ensure consistent drive point excitation locations. When the test was set back up, the same bungee cords were used to suspend the test article, and the stinger was simply re-attached to the force gauge that was left attached to the test article.

The laser head was positioned approximately 1.26 m (49.9 in) from the test article. Four scans were used for this test to measure all sides of the test article. A similar alignment scheme was used for this test, utilizing the ring of holes and tip of the test article as alignment points. The error in the alignment for this test was on average 2.6 mm, which is twice the value of the previous test. Note that this should not imply that the newer system is somehow less accurate than the baseline system: the alignment process depends greatly on operator interaction and test setup. Given the uncertainty in placing the alignment

points on the test article and the spacing of the test grid, both of these alignments were considered 'good enough' and no further improvement in the alignment was sought.

For this test, the frequency resolution was increased to try to better separate the repeated modes. The bandwidth was set to 2,500 Hz with a frequency resolution of 0.78 Hz. Pseudorandom excitation was used for this test, so only five averages were used and no windows were applied. All signal enhancement parameters were set to their highest levels.

During testing it was immediately obvious that significant improvements had been made between the newer SLDV system and the previous generation system. The laser was able to measure clean frequency response functions at up to six circumferential stations at a time (see Figure 8), at angles of incidence up to 66 degrees from the surface normal. The new system also had much less difficulty measuring on the darker surface, and was able to measure relatively clean FRFs at high AoI as shown in Figure 9.

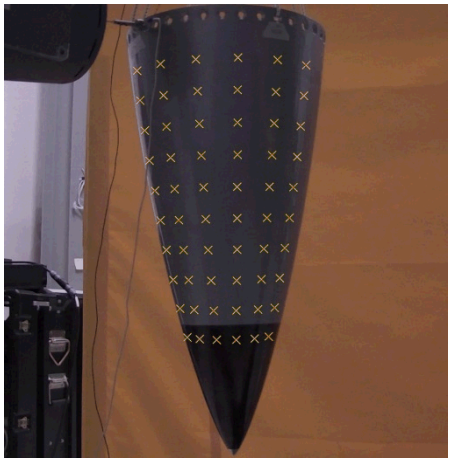

Figure 8: Laser camera view showing measurement points for one scan.

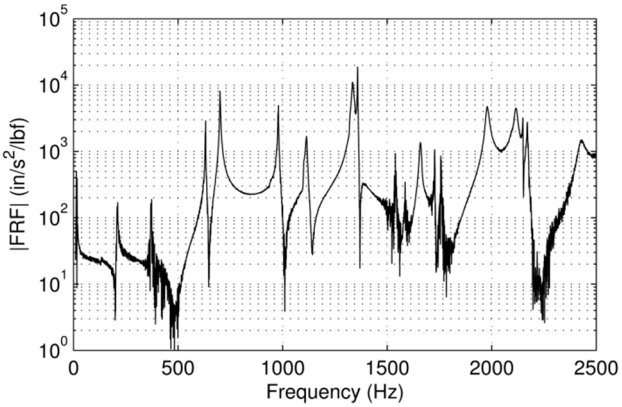

Figure 9: FRF measured with the new SLDV system in 1D mode on the darker surface at an AoI of 66 degrees.

2.3 3D Test with New System

After the 1D test with the new system, a 3D test was performed. The laser heads were placed an average of 1.42 m (56.1 in) from the test article. The average separation between two laser heads was 0.649 m (25.5 in). Figure 10 shows an example setup. Each laser head was individually aligned with features on the part as described in Section 2. The average error in the alignment was 2.0 mm. Four measurements were required to scan all sides of the test article.

Figure 10: 3D test setup

Because there were no markings on the part to designate measurement points, it was difficult to determine the alignment error during the 1D scans at points other than those used to set the alignment (e.g. Figure 5). There was no reference point to measure the laser positioning against at any given measurement point; unless the laser spot was so far from the correct measurement point that it was obviously misplaced, it was impossible to draw any kind of conclusions about measurement point uncertainty. With the 3D measurement, one can get an idea of the position error due to the error in the alignment of the laser spots.

When the lasers are perfectly aligned, the laser spots should be exactly on top of one another on any point on the test article's surface. However, if the lasers have some alignment error, the laser spots will generally appear as three distinct points. This effect will become more pronounced at a higher AoI to the test article, as the same angular misalignment will result in a greater displacement of the spot along the surface. One can use the spread of these points as an estimate for the error in the measurement point locations. Figure 11 shows two examples of spot misalignment during the laser scan.

To correct this misalignment, a technique known as video triangulation was used. This technique detects each laser spot on the laser camera image and moves the lasers so the spots are collocated. This technique was very helpful to get the laser spots to converge on one point, as the alignment could not be easily improved.

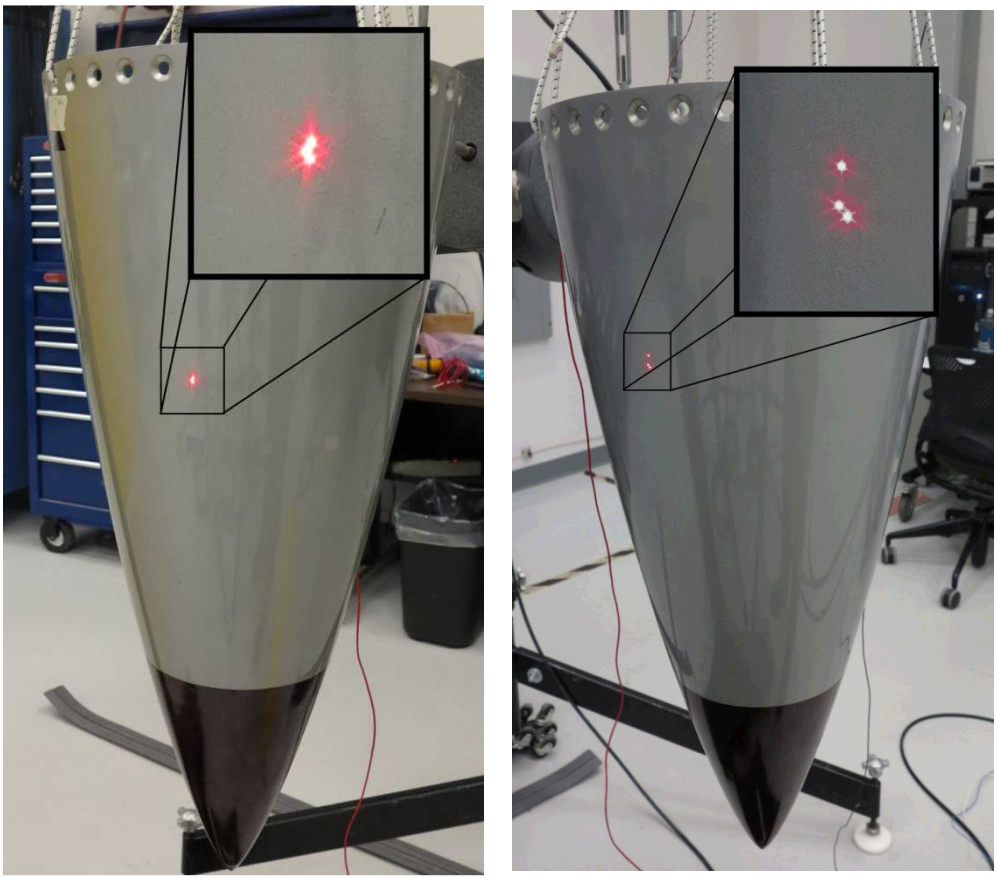

Figure 11: Misalignment of laser spots at small AoI (left) and at large AoI (right).

This test used the same data acquisition parameters as the 1D test in Section 2.2. The bandwidth was set to 2,500 Hz with a frequency resolution of 0.78 Hz. Pseudorandom excitation was used for this test, so only five averages were used and no windows were applied. All signal enhancement parameters were set to their highest levels.

3 ANALYSIS AND COMPARISONS

Often times with plate-like structures with the laser system sufficiently far away, it is an adequate assumption to assume that all of the measurements are perpendicular to the surface; however, for this test the laser beams formed angles over 50 degrees with the test article's surface normal direction, so that assumption would not be valid. For each of the 1D tests, the test geometry needed to be updated so the measurement coordinate systems matched the actual direction of measurement.

A coordinate system was assigned to each measurement point based on that point's position in space and the laser head's origin. The local *z* axis, denoted by the unit vector $\hat{\mathbf{z}}$, was defined as the vector from the measurement point (located at $\mathbf{p}_n$) to the laser's origin (located at $\mathbf{p}_o$). The local *x* and *y* axes were then placed orthogonal to one another and the local *z* axis, with the *x* axis pointing away from the tip of the test article towards the global *x* direction. This was achieved by defining the local *y* axis, denoted by the unit vector $\hat{\mathbf{y}}$, as the cross product between the local *z* axis and the global *x* axis, denoted by the unit vector $\hat{\mathbf{X}}$. Finally, the local *x* direction, denoted by $\hat{\mathbf{x}}$, was defined as the cross product between the local *y* and *z* directions. A transformation matrix $\mathbf{T}$ could then be formed from the local axes. These computations are shown in (1)-(6). Figure 12 shows the measurement directions for the baseline test.

$$\mathbf{z} = \mathbf{p}_o - \mathbf{p}_n \tag{1}$$

$$\hat{\mathbf{z}} = \frac{\mathbf{z}}{\|\mathbf{z}\|} \tag{2}$$

$$\mathbf{y} = \hat{\mathbf{z}} \times \hat{\mathbf{X}} \tag{3}$$

$$\hat{\mathbf{y}} = \frac{\mathbf{y}}{\|\mathbf{y}\|} \tag{4}$$

$$\hat{\mathbf{x}} = \hat{\mathbf{y}} \times \hat{\mathbf{z}} \tag{5}$$

$$\mathbf{T} = \begin{bmatrix} \mathbf{x}^T \\ \mathbf{y}^T \\ \mathbf{z}^T \end{bmatrix} \tag{6}$$

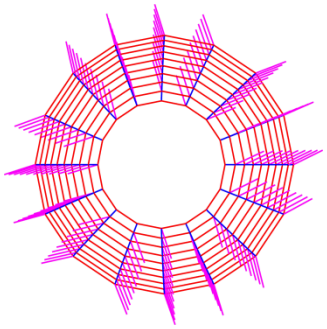

Figure 12: Example measurement vectors for the baseline test.

3.1 Frequency Response Function Comparisons

Data were then compared between the baseline test using the previous generation laser hardware and 1D test using the current generation laser hardware. Because the test setup had to be dismantled between the baseline and 1D tests, there were differences in the positioning of the laser head with respect to the test article between the two tests. FRF comparisons between the two tests were only made at points where the measurement vectors were within 10 degrees of one another. Except for cases of modes shifting between the tests (which will be discussed in Section 3.2), the frequency response functions show good agreement on the lighter grey surface; however, the baseline data is significantly noisier for the darker surface. These comparisons are shown in Figure 13. Many points on the darker surface were not able to be measured with the baseline system due to the high rate of signal dropouts which would cause over-ranges of the data acquisition system.

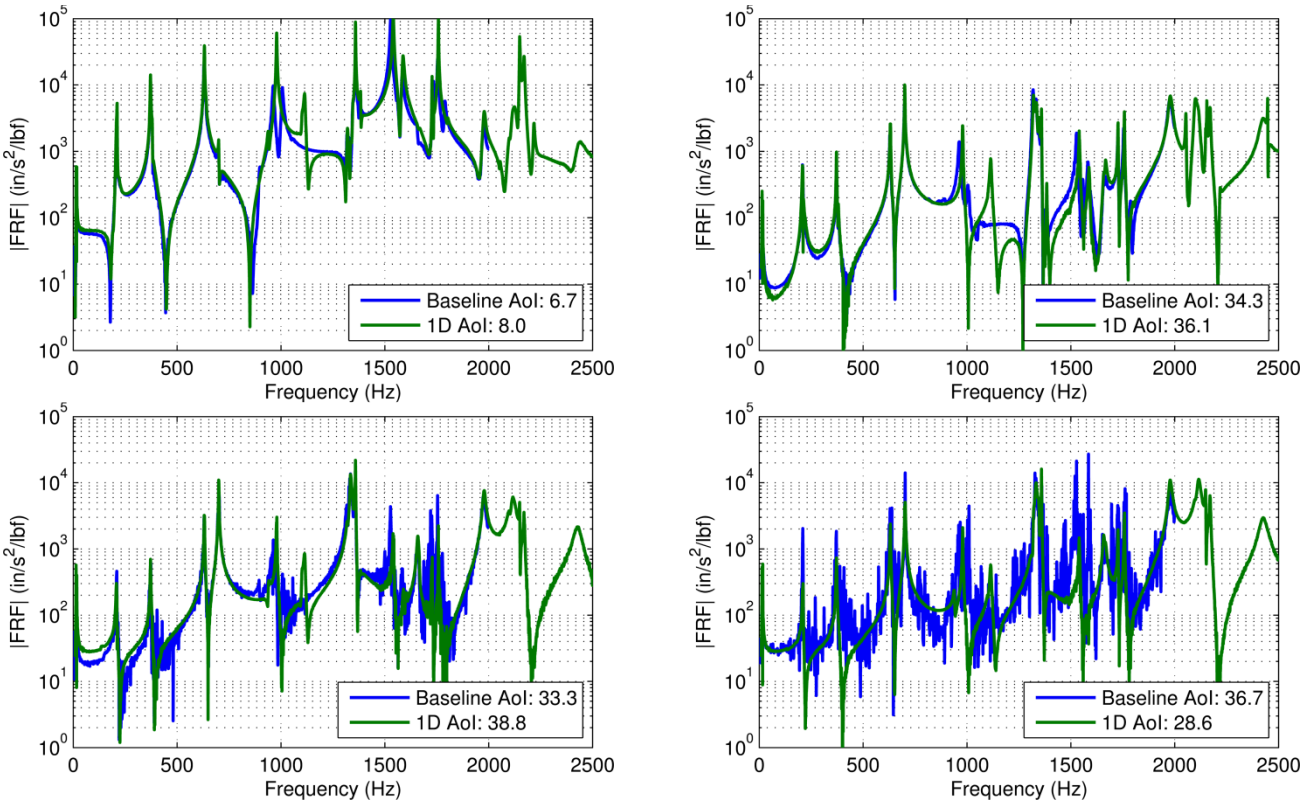

Figure 13: Frequency response function comparison for two points on the lighter surface (top) and two points on the darker surface (bottom).

3.2 Mode Shape Comparisons

Modes were fit to each data set using the SMAC algorithm [2]. Due to the symmetry of the structure, a number of mode pairs were present, but it was often difficult to extract both modes because only one input location was used. Often SMAC would converge on both modes, but one would have a negative drive point coefficient, so it would be discarded. Generally good fits to the experimental data were achieved. A complex mode indicator function (CMIF) is shown for each test in Figure 14, and the extracted modal parameters are listed in Table 1.

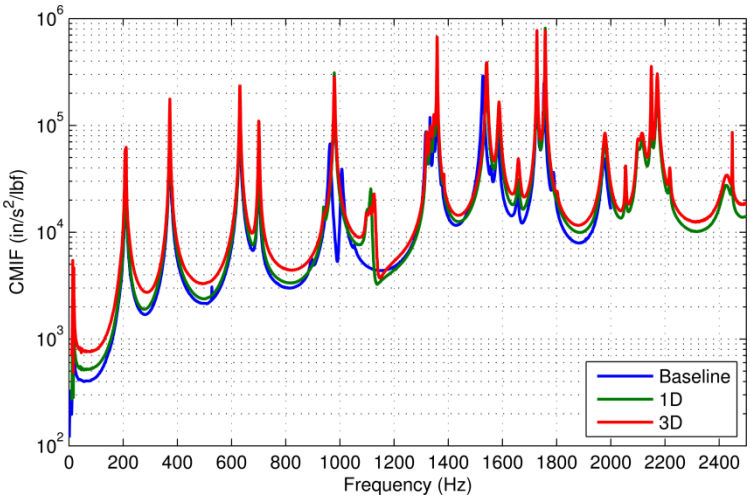

Figure 14: CMIFs for the three tests.

Table 1: Extracted modes from the three tests. Modes 11 through 13 are thought to be due to false stinger modes.

Mode	Baseline Test		1D Test		3D Test		Description
	Frequency (Hz)	Damping Ratio	Frequency (Hz)	Damping Ratio	Frequency (Hz)	Damping Ratio	
1	209.1	0.69%	208.8	0.90%	208.2	0.88%	First 2-lobed Ovaling
2	--	--	--	--	211.4	0.24%	Pair with Mode 1
3	371.9	0.40%	372.4	0.30%	372.5	0.25%	First 3-lobed Ovaling
4	381.3	0.34%	381.1	0.28%	381.3	0.23%	Pair with Mode 3
5	630.5	0.19%	631.3	0.18%	631.1	0.17%	First 4-lobed Ovaling
6	640.2	0.29%	--	--	--	--	Pair with Mode 5
7	700.9	0.25%	701.0	0.18%	701.1	0.18%	Second 2-lobed Ovaling
8	--	--	--	--	703.2	0.16%	Pair with Mode 7
9	--	--	940.0	0.29%	940.8	0.86%	First 5-lobed Ovaling
10	963.0	0.32%	979.4	0.15%	980.0	0.17%	Pair with Mode 9
11	1007	0.35%	1099	0.30%	1098	0.57%	5-lobed Ovaling*
12	--	--	1115	0.25%	1114	0.35%	Pair with Mode 11*
13	--	--	--	--	1127	0.47%	Pair with Mode 11*
14	1317	0.20%	1320	0.19%	1320	0.19%	Second 3-lobed Ovaling
15	1331	0.26%	1332	0.29%	1333	0.29%	Third 2-lobed Ovaling
16	1334	0.32%	1335	0.32%	1336	0.33%	Pair with Mode 15
17	1345	0.21%	1347	0.18%	1347	0.19%	Pair with mode 14
18	1358	0.09%	1359	0.04%	1359	0.05%	First 6-lobed Ovaling
19	1528	0.15%	1541	0.15%	1542	0.16%	Second 5-lobed Ovaling
20	1558	0.13%	--	--	--	--	Pair with mode 19
21	1583	0.23%	1587	0.23%	1587	0.24%	Second 4-lobed Ovaling
22	1593	0.16%	--	--	--	--	Pair with mode 21
23	1657	0.27%	1659	0.26%	1659	0.26%	First Bending
24	--	--	1667	0.25%	1667	0.26%	Pair with mode 23
25	1727	0.09%	1727	0.05%	1727	0.04%	7-lobed Ovaling
26	1755	0.10%	1758	0.04%	1758	0.06%	6-lobed Ovaling
27	1788	0.20%	1802	0.16%	1802	0.16%	6-lobed Ovaling
28	1975	0.37%	1978	0.34%	1979	0.39%	Third 3-lobed Ovaling
29	--	--	2054	0.08%	2054	0.08%	5-lobed Ovaling of Tip
30	--	--	2055	0.09%	2056	0.07%	Pair with mode 29
31	--	--	2099	0.24%	2099	0.25%	4-lobed Ovaling of Tip
32	--	--	2116	0.39%	2116	0.40%	Fourth 3-lobed Ovaling
33	--	--	2149	0.04%	2124	0.49%	Pair with Mode 32
34	--	--	2172	0.13%	2150	0.04%	8-lobed Ovaling
35	--	--	2218	0.12%	2172	0.13%	Higher-order Ovaling
36	--	--	2428	0.74%	2218	0.12%	Higher-order Ovaling
37	--	--	--	--	2427	0.66%	Fifth 3-lobed Ovaling

To compare the shapes between the different tests, common degrees of freedom needed be used, but all three tests used different local coordinate systems at the measurement points. Since the 3D test had data for all three directions, it could be transformed into coordinate systems consistent with the baseline and 1D tests using the **T** matrix from (6) at each measurement location. After the data were transformed, they were reduced to the one-dimensional measurements from the baseline and 1D tests. The modal assurance criterion (MAC) matrix could then be computed between the three data sets, as shown in Figure 15. High off-diagonal values were found between the modes from 940-1127 Hz.

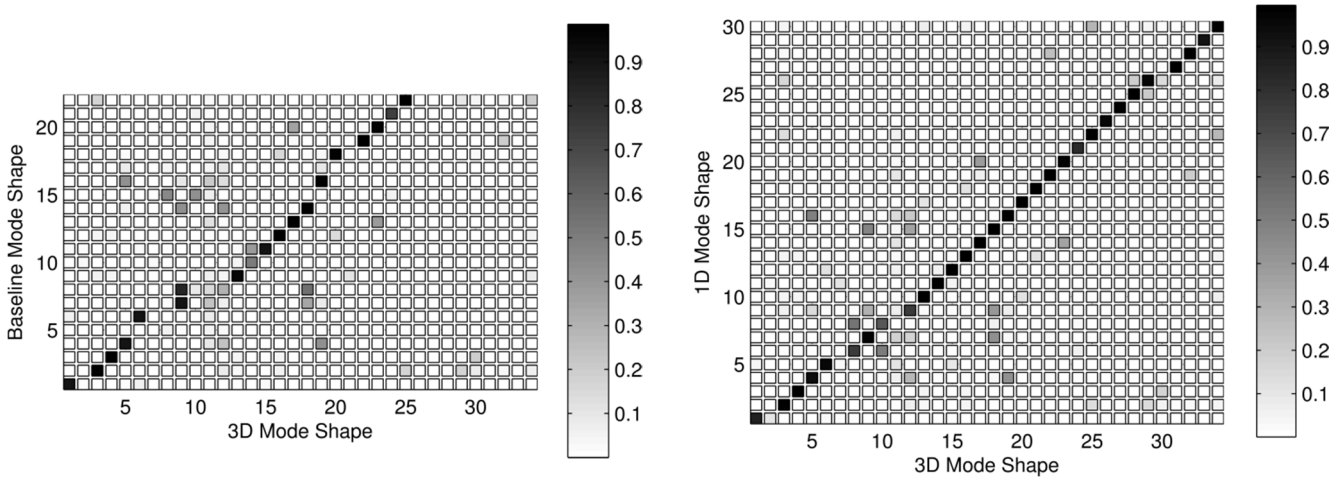

Figure 15: MAC matrices showing mapping between extracted modes.

The CMIF in Figure 14 and fits in Table 1 show good agreement between the three tests for the majority of natural frequencies. Due to the increased frequency resolution and bandwidth, the 1D and 3D tests found modes that were not found in the baseline test; however other interesting differences were noted as well, particularly in the 5-lobed ovaling modes from 900-1150 Hz. While the mode shapes matched very well between the three tests, these modes showed a large change in frequency between baseline test and the other two tests. Some small change in the modal parameters may be expected between the two tests because the test setup was dismantled between the baseline test and the subsequent tests, an approximately 100 Hz shift indicates issues other than minor differences in boundary conditions.

Another observation which raised suspicion regarding these modes was that a significant shift in natural frequency occurred between laser scans for the three modes near 1100 Hz. This was discovered while fitting modes to the 3D test: the SMAC algorithm fit three modes for the 5-lobed ovaling modes near 1100 Hz, but generally these types of modes should appear in pairs. The second and third mode of this group each looked like half a mode shape, as shown in Figure 16, and the CMIF computed from the FRFs from each of the four scans in the 3D test showed a distinct shift between the four scans, shown in Figure 17.

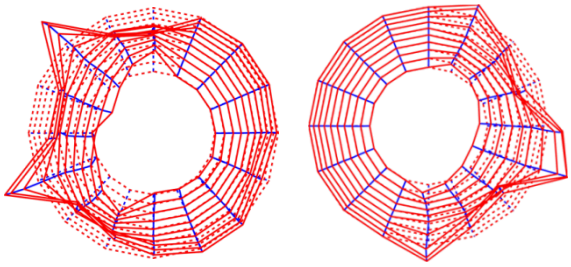

Figure 16: Two extracted mode shapes each having motion on one half of the shape.

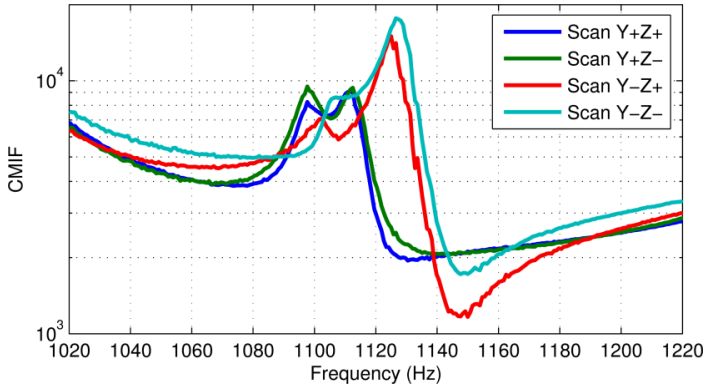

Figure 17: Complex mode indicator function showing a shift in frequency between scans taken approximately two hours apart.

The shift in the natural frequencies between two scans taken two hours apart raised a great deal of suspicion about the validity of this set of modes. The suspension of the test article did not change during this time, so significant changes in natural frequency were not expected. The stinger and shaker hardware was therefore investigated as the culprit. The shaker and force gauge were removed from the test article and a drive point measurement was performed using a modal hammer, and the measured drive point FRF is shown in Figure 18. The hammer data suggests that the group of modes near 1100 Hz extracted from the 1D and 3D scans are indeed false modes. Additionally, the mode near 980 Hz was split into two peaks in the baseline test, similar to a tuned vibration absorber like what was seen in [3]. The hammer impact data also showed somewhat higher natural frequencies, likely due to the removal of the relatively massive force gauge from the relatively thin shell structure. This suggests that mass-loading may also be an issue during these tests.

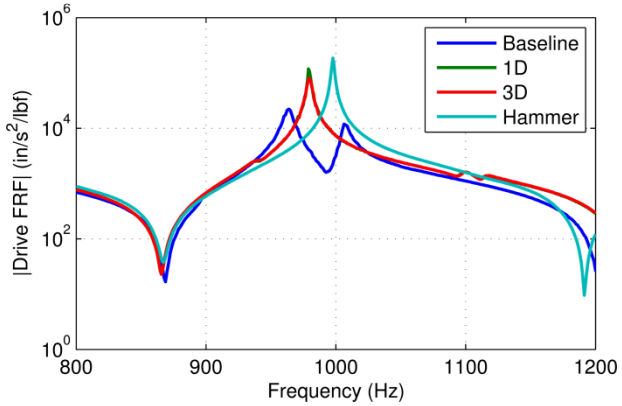

Figure 18: Drive point FRF showing the three tests compared to a hammer impact near the suspicious modes.

4 LESSONS LEARNED

The tests described in this report were helpful in understanding the capabilities and improvements of the new 3D SLDV system. The new system was able to get better signal return off of both surfaces tested, and was able to make adequate measurements even on the dark surfaces and at high angles of incidence with the structure. Adding to that the capability to make 3D measurements at a large number of points, the new system was seen as a substantial improvement over the previous generation system owned by Sandia National Laboratories.

This test also identified areas of improvement for testing with the 3D SLDV system. The lasers were aligned with what few features were available on the part; however, these features were not sharp points but were instead broad features that introduced uncertainty into the alignment. For a number of points, the laser spots were not collocated and appeared as three distinct spots on the test article. Video triangulation of the laser spots was successful for this test article, but future test articles may not be as successful due to sharp edges or reflective surface finishes. In tests performed since this investigation, a reference object with features at known coordinates has been used to align the laser heads accurately. Subsequently, then a coordinate transformation is applied to transform from the reference object's coordinate system to the test article's coordinate system. This way, even if there is uncertainty in the locations of the points used to transform between coordinate systems, the relative positions of the laser heads within that coordinate system will still be accurate, which lets the laser beams converge at any point in space.

Another area of improvement was reducing mass loading and shaker effects. SLDV has the advantage over traditional sensors in that it is non-contact and does not mass load the part. However, it would seem that this test suffered from both contact issues (coupling with the shaker stinger to produce false modes) and mass loading issues (significant shifts in natural frequency between hammer and shaker input). Accordingly, more effort and investment have been put into excitation methods that have a less significant impact on the structure, especially as smaller articles are tested. Smaller force transducers have since been purchased, and impact testing has been successfully used on a number of test articles since this test was performed.

Impact testing with the 3D SLDV system has its own challenges that need to be addressed. Some type of automatic hammer is desirable for SLDV testing due to the large number of impacts that are sometimes required. These hammers can be inconsistent, and often times they are not designed for frequent impacts over long durations. This can increase testing time as the automatic hammer may require time to cool down between impacts. Additionally hammers often impart large rigid body deflections on the test article, and this can reduce the accuracy of SLDV tests as the part moves with respect to the fixed laser spot. Hammer testing has been successful by using a smaller hammer that is swung by the automatic hammer, as shown in

Figure 19. The smaller hammer is then partially decoupled from the inertia of the automatic hammer, and this imparts less rigid body motion and leads to shorter ring-down times.

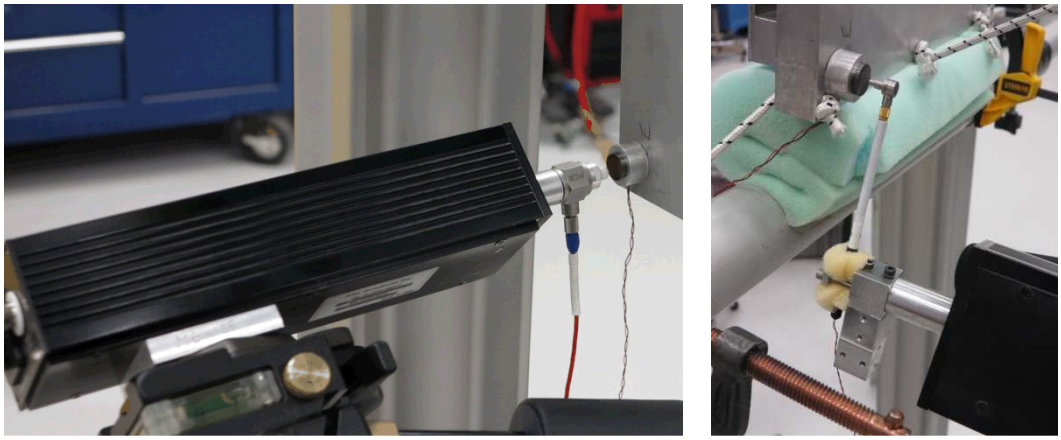

Figure 19: Automatic hammers for impact testing with SLDV.

5 CONCLUSIONS

A series of modal tests were performed on a conical test article with two surface finishes to identify the capabilities of a newly purchased 3D SLDV system. The new SLDV system performed significantly better than the previous generation system and was able to produce clean FRFs at high angle of incidences and on dark surfaces. During modal analysis, it was found that the shaker hardware that was used to excite the test article produced false modes and imparted mass loading effects. These were identified by performing a quick hammer tap test and comparing drive point frequency response functions.

This investigation allowed test personnel to gain experience with using the new 3D SLDV system and identify gaps in the capability that could be improved for production tests. Alignment procedures and excitation methods have since been improved, and a number of production articles have been tested successfully.

6 REFERENCES

[1] Castellini, P., Martarelli, M., and Tomasini, E.P., "Laser Doppler Vibrometry: Development of advanced solutions answering to technology's needs", *Mechanical Systems and Signal Processing*, Volume 20, Issue 6, p. 1265-1285, 2006.

[2] Hensley, Daniel P., and Mayes, Randall L., "Extending SMAC to Multiple References", *Proceedings of the 24th International Modal Analysis Conference,* pp.220-230, February 2006.

[3] Avitabile, Peter, "Back to Basics". *Experimental Techniques*, Volume 29, Issue 6, p. 23-24, 2006.